Macromolecules

pubs.acs.org/Macromolecules Article

Exploring Morphological Effects on the Mechanics of Blended Poly(lactic acid)/Poly(ε-caprolactone) Extruded Fibers Fabricated Using Multilayer Coextrusion

Kris M. Van de Voorde, Jonathan K. Pokorski,* and LaShanda T. J. Korley*

Cite This: https://dx.doi.org/10.1021/acs.macromol.0c00289 Read Online

ACCESS | Metrics & More | Article Recommendations | Supporting Information

ABSTRACT: Nanofibrous materials composed of polyesters play a key role in several technologically demanding fields, most notably that of biomedicine. A critical feature of polyesters is their ability to tune mechanical properties through simple blending of components. This work explores the fabrication of blended poly(lactic acid)/poly(ε-caprolactone) (PLA/PCL) fibers manufactured through multilayer coextrusion. Morphology, crystallinity, and crystallite size were probed for a continuum of blends to understand the resultant mechanics of the nanofibers. Fibers with differential weight ratios displayed a droplet-in-matrix morphology (75/25 PLA/PCL; 25/75 PLA/PCL), whereas 50/50 PLA/PCL blends exhibited a cocontinuous morphology. Depression of the crystallinity of both phases was observed for all blends and changes in the mean crystallite size typically decreased upon blending. The microscale behavior of the materials explains the tensile properties of the fibers; mechanical analysis showed that the addition of PCL increased the extensibility and toughness, in particular, for blends that formed a cocontinuous morphology. Correlating morphological effects on the crystallinity and mechanics of melt-processed fibers provides insight into the interaction between two semicrystalline phases and provides valuable insight for future technological development.

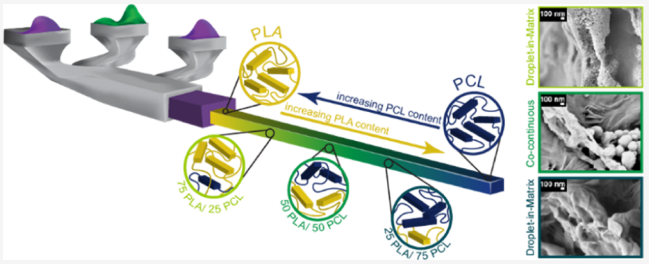

INTRODUCTION

Blending of dissimilar polymers provides an economical and efficient pathway to tune material properties, such as mechanics,[1] barrier properties,[2] processability,[3] and degradation rate.[4] For example, a brittle polymer can be toughened through mixing with a rubbery counterpart.[5] However, the majority of polymer blends are immiscible because of dissimilar backbone structures, causing unfavorable enthalpies of mixing and leading to heterogeneous materials with spatial separation between phases.[6] Understanding and controlling the microstructure of this phase separation often dictates the mechanical properties of blended polymers.

Polyesters are excellent candidates for blending approaches because of their range of mechanical properties and their great technological utility.[7] For example, polyesters are appealing for many biomedical applications, such as tissue engineering, because of their wide range of mechanical profiles and their tunable hydrolytic degradation rates.[8] One example of a commonly fabricated immiscible polyester blend is that of poly(lactic acid) (PLA) and poly(ε-caprolactone) (PCL).[9] These specific polyesters are often blended together because of their complementary characteristics. PLA offers robust mechanical strength with limited ductility and undergoes rapid hydrolytic degradation.[10] By contrast, PCL is ductile with poor mechanical strength and longer degradation time frames.[11] A recent study highlights the utility of blending PCL and PLA, where it was determined that the toughness of a PLA material could be increased over 10-fold when blended with 20 wt % PCL.[12] Consequently, by blending these two materials, facile tuning of the mechanical properties was enabled.

Beyond manipulating the mechanical characteristics of a given polymer blend, controlling the nano/microscale morphology of materials is important when designing for specific applications.[13] In tissue engineering, nanofibrous scaffolds are particularly advantageous because their highly porous nature allows for nutrient influx and waste efflux.[14] One of the most common nanofiber fabrication methods is electrospinning, typically a solvent-based process.[15] In electrospinning, polymer concentration, solvent type, flow rate, voltage, and tip-to-collector distance are key parameters that must be balanced to achieve target cross-sectional diameters and regularity in fiber shape.[16] The electrospinning process has drawbacks such as sensitivity to environmental factors, like humidity, and is performed in batch mode at relatively low

Received: February 5, 2020
Revised: May 22, 2020

throughput.[17] PLA/PCL blended fibers fabricated via electrospinning have been studied extensively, primarily focusing on the manipulation of mechanics and degradation rate.[18,19]

Recently, a scalable and reproducible fiber fabrication process, multilayer coextrusion, has emerged, which relies on continuous melt-based processing methods.[6,16,17] This manufacturing technique comprises four process steps within the extrusion line. In brief, two immiscible polymer melts (Figure 1) are fed through two single-screw extruders and coextruded into a rectangular barrel, such that the two melts are horizontally separated (step I). The melts are then flowed through a series of vertical multipliers that split and stack the melt flow to form vertically aligned layers (step II). Next, a polymer skin layer is pumped onto the top and bottom of the polymer melt (step III). Lastly, the flow passes through a series of horizontal multipliers that split and stack the melt (step IV) prior to the extrudate's exit from the die. The resulting product is a composite tape, consisting of continuous rectangular fibers (green and red) embedded within a sacrificial matrix (purple). The domain sizes of the fibrous components are geometrically controlled by the number of multiplication steps present in steps II and IV and can vary from ∼100 nm to several microns in cross-section. Subsequently, fibers can be isolated from the composite tapes *via* a high-pressure water washing step that delaminates the fiber domains from the sacrificial matrix component, forming a nonwoven fiber mat. The advantages of this approach are numerous and include high-throughput fabrication (∼1.5 kg h^{-1} of composite tape) and flexibility to produce single- or dual-component fibers from a variety of melt-processable polymers. Additionally, these rectangular-cross-section fibers have a much higher surface-area-to-volume ratio than typical cylindrical fibers. This higher surface is advantageous when designing materials, such as tissue-engineered scaffolds, to enable better cellular proliferation.[14]

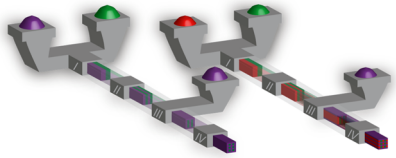

Figure 1. Overview of the multilayer coextrusion process. Left: two-component system. Right: three-component system. Composite tapes are fabricated through a four-step process. Initially, (step I) two immiscible polymer melts are coextruded. The melts then pass through a series of vertical multipliers (step II). A skin layer is added to the top and bottom of the melt (step III). Lastly, the polymers flow through a series of horizontal multipliers (step IV), and a composite tape is produced.

The unique method used to produce these fibers enables a wide range of postprocessing strategies to manipulate mechanical properties, supporting applications in medicine or filtration.[15,20] For example, a postprocess drawing step was able to enhance crystallinity and achieve controlled alignment of crystalline and amorphous domains within PCL fibers, thus increasing the modulus of the fiber by an order of magnitude.[18,19] Extruded PCL fiber scaffolds have also been utilized as substrates for fibroblast and neural cell differentiation upon surface modification with peptides known to induce differentiation.[14,16] Furthermore, these fibers can be coalesced into nonwoven fabrics which have been applied to the biologically triggered release of growth factors for use in smart wound-healing patches and in antifouling filters.[20,21]

Blending of multiple polymers into individual fibers to achieve differential mechanical properties is yet to be explored in multilayer coextrusion technology. In this work, we extend the technological impact of multilayer coextrusion to fabricate extruded fibers composed of two semicrystalline polyesters with complementary mechanical properties and varying degradation profiles. In this investigation, PLA (rigid) and PCL (elastomeric) are coextruded to form the fibrous domains in multilayer composites. Using multilayer coextrusion as the processing platform to manufacture PLA/PCL fiber blends, the connection between morphology, crystallinity, and fiber mechanics as a function of blend composition is detailed in this work. These findings will enable the design of fiber scaffolds with tunable degradation profiles and controlled mechanics suitable for application spaces in biomedicine and agriculture.

EXPERIMENTAL SECTION

Processing of Composite Tapes. PLA was purchased from Nature Works (INGEO BIOPOLYMER 2003D, 155 kg/mol[21]), and PCL was purchased through The Perstorp Group (CAPA 6800, 87 kg/mol[21]). PLA and PCL were blended at 160 °C in a corotating twin-screw extruder (W&P 25k-30) having a screw length to diameter ratio of 28.5 and then dried under vacuum for 24 h at 40 °C. Three different formulations (based upon wt %) were blended as the fiber component of the composite tapes 75 PLA/25 PCL, 50 PLA/50 PCL, and 25 PLA/75 PCL. To form the matrix component of the composite tape, two poly(ethylene oxide) (PEO) powders were purchased from Dow, having two different molecular weights (100 and 200 kg/mol), and were melt-blended at 160 °C at a weight ratio of 70:30 (POLYOX WSRN-10:POLYOX WSRN-80). This approach was followed to match the viscosity of the PEO with that of the PLA/PCL blend during multilayer coextrusion, as previously described.[18]

Once the blended filaments were pelletized, the materials were again dried at 40 °C for 48 h under vacuum in preparation for multilayer coextrusion. The temperature of a 3/4 inch single-screw extruder was set to 200 °C so that all three components used (PLA, PCL, and PEO) had the same viscosity during processing. The residence time was 25 min. The extruder was outfitted with 16 vertical multipliers and 4 horizontal multipliers, and a 33% PEO skin layer was added to the top and bottom of the vertically layered melt to yield composite tapes containing continuous PLA/PCL blend fiber domains in a PEO matrix. Additionally, the pump rate of the extruders was set to a 1:1 ratio while rotating at 15 rpm. The composite extrudate was formed using a 1 inch tape die and collected on a steel chill roller rotating at 30 rpm, yielding a composite tape containing 1024 individual, continuous polyester fiber domains. A belt conveyer was used to collect the material to ensure that the material cooled without inducing preferential chain orientation.

Isolating Fibers. The PLA/PCL fibers were isolated from the PEO matrix *via* a three-step process (Figure 2a). Initially, the composites were secured across beakers and submerged in a methanol/water (70:30% by volume) bath for 24 h. Next, delamination of the extruded fibers was achieved utilizing a custom high-pressure (3.45 MPa) water jet equipped with a 0.24 mm diameter nozzle, purchased from Atomizing Systems, Inc. Finally, to remove residual PEO, the fibers were again placed in an agitated bath of water and methanol for 96 h to yield nonwoven fiber mats (Figure S1). After the final wash, the PCL/PLA blended fibers were dissolved in deuterated chloroform ($CDCl_3$) overnight, and ^1H NMR (Bruker 600 MHz) spectroscopy was utilized to quantify PLA/PCL wt % (S11).

Imaging Fibers. To confirm fiber architecture and determine fiber dimensions, scanning electron microscopy (SEM, Jeol JSM-7400F) was conducted utilizing an accelerating voltage of 3 kV. The isolated

https://dx.doi.org/10.1021/acs.macromol.0c00289
Macromolecules XXXX, XXX, XXX−XXX

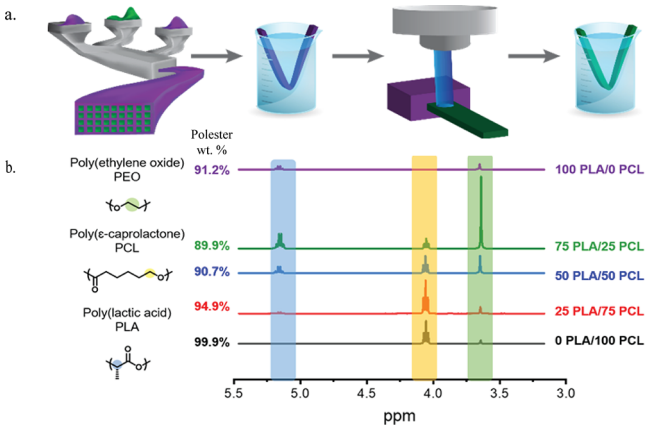

Figure 2. (a) Schematic representation of the extrusion-wash−delaminate-wash process. Here, the polyester fibers (green) are coextruded alongside PEO (purple) to form a composite tape. To isolate the fibers from the matrix, tapes are placed in a water and methanol bath for 24 h and subjected to a high-pressure water jet. To remove the remaining PEO, the fibers are again placed in a water and methanol bath for 96 h. (b) Analysis of ^{1}H NMR after the fiber isolation process. Relative integration values were calculated, and it was determined that the isolated fibers were >89.9% polyester.

fibers were mounted on a sample stage and sputter-coated with a layer of Au/Pd prior to imaging. ImageJ software was used to measure the width and thickness of the PLA/PCL fibers, and the fiber dimensions were calculated from an average of 50 measurements (Figure S2).

To examine the blend morphology, the PLA/PCL fibers (25/75, 50/50, and 75/25) were etched to selectively remove one phase. For the 75/25 and 50/50 PLA/PCL blended fibers, the PCL phase was etched by exposing the fibers to a tetrahydrofuran (THF) atmosphere for 25 min. For the 25 PLA/75 PCL blend, the PLA phase was selectively removed by immersing the fibers in acetic acid for 1 min. After the etching process was complete, the PLA/PCL fibers were washed with methanol and dried under vacuum overnight prior to SEM analysis.

Thermal Properties. Dynamic scanning calorimetry (DSC, TA Discovery Series) was utilized to examine the thermal behavior of the PLA/PCL fiber blends. Thermal transitions were determined from nonwoven fiber samples sealed in hermetic pans, using a blank hermetic pan as a reference under a nitrogen atmosphere. The samples were initially cooled and held at 0 °C for 3 min to equilibrate and then heated to 200 °C at 10 °C/min before cooling down to 0 °C at 10 °C/min. The melting temperature (T_m) was measured at the endothermic peak, and the crystallization temperature (T_c) was measured at the exothermic peak. The percent crystallinity (X_c) for PLA and PCL was calculated from the DSC melting enthalpies (eq 1) using a value of 75.6 J/g for 100% crystalline PLA[22] and 139 J/g for PCL.[23] Additionally, the wt % (w) was included while measuring the crystallinity and the cold crystallization enthalpy (ΔH_c) for PLA blends.

$$X_c = \frac{(\Delta H_f - \Delta H_c)}{w\Delta H_f^{\circ}} \quad (1)$$

Wide-Angle X-ray Scattering. Fibrous samples were mounted on a sample stage, and wide-angle X-ray scattering (WAXS) data were collected on a Xenocs Xeuss 2.0. A CCD detector with a pixel resolution of 486 × 618 (1 pixel = 0.172 cm) was used to collect the scattered beam. X-rays (1.542 Å wavelength) were generated at 50 kV. Fibers were exposed to the beam for 15 min at a sample-to-detector distance of 800 cm. Silver behenate was used to calibrate the instrument, and the data sets were corrected for background noise and sample absorption. Azimuthal averaging was performed to obtain intensity as a function of the scattering vector, q. To process the data, Origin 8.1 was utilized, and the peaks were fit using a Lorentzian function.

Tensile Measurements. Cross-sectional areas of the fibers were measured using a micrometer and corrected for porosity by deducting the void fraction (Table S1). Nonwoven polyester fiber mats of similar dimensions and mass were loaded between Teflon clamps such that the average directionality of the fibers was parallel to the clamp direction.

A Zwick/Roell mechanical testing instrument equipped with a 100 N load cell was utilized to perform the uniaxial tensile test at 50% min^{-1} at room temperature. Each specimen was tested a minimum of five times per sample, and failure was determined when 90% of the maximum force was lost.

RESULTS AND DISCUSSION

Fiber Isolation and Imaging. To fabricate blended polyester fibers, whose mechanical properties and degradation rates could be tuned, PLA and PCL were compounded in varying weight percentages prior to multilayer fiber fabrication (25/75, 50/50, 75/25; PLA/PCL). Each compound blend and virgin polyesters (PLA and PCL) were coextruded with PEO such that a composite tape was manufactured where PLA/PCL fibers were embedded in a PEO matrix. Isolation of the fibers was accomplished through a three-step washing−delamination−washing procedure designed to dissolve the PEO matrix, while leaving the PLA/PCL fibers unchanged (Figure 2a).

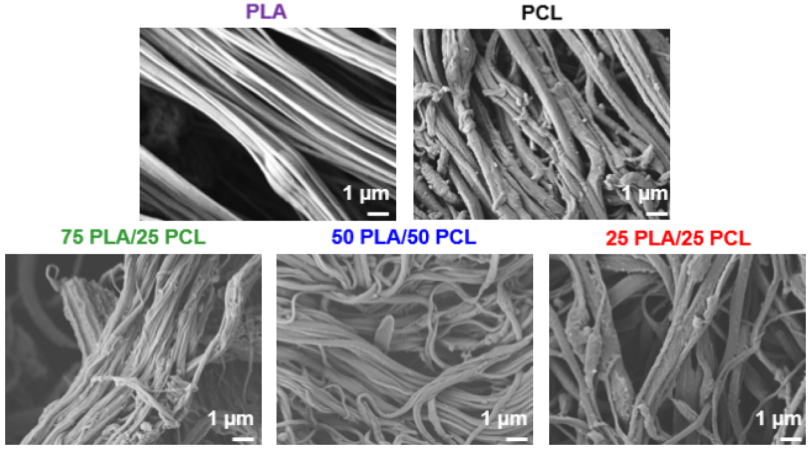

Figure 3. SEM micrographs of the extruded PLA/PCL fibers. The control PLA and PCL and blended PLA/PCL fibers were rectangular in shape without surface texture.

https://dx.doi.org/10.1021/acs.macromol.0c00289
Macromolecules XXXX, XXX, XXX−XXX

Utilizing ^{1}H NMR spectroscopy, the relative weight fraction of PLA and PCL was calculated. Peak characteristics of PEO, PLA, and PCL at 3.7, 5.1, and 4.1 ppm, respectively, were integrated to provide the PEO/polyester content ratio, and a minimum of 89.9 wt % polyester fibers was achieved (Figure 2b). Because of the partial miscibility of PLA and PEO,[24] the control PLA fibers and the 75 PLA/25 PCL fiber blend contained a higher weight fraction of PEO.

Once the control (PCL and PLA) and blended PLA/PCL extruded fibers were isolated from the PEO matrix to form nonwoven mats, the fiber architecture and dimensions were examined *via* SEM (Figure 3). As expected, rectangular fibers were observed and found to be similar to the single-component fibers obtained in prior studies.[14,25,26] Gratifyingly, the surfaces of the blended PLA/PCL fibers appeared smooth, indicating that the morphology of the blends did not induce surface texturing.[27] This observation is particularly noteworthy as solvent-based, fiber-processing techniques may induce surface effects.[28]

To probe the dimensions of the fibers as a function of composition, SEM images were analyzed using ImageJ software (Table 1). The control and PLA/PCL extruded fibers were found to have similar widths (~300 nm) and thicknesses (~200 nm). Given that each PLA/PCL system was extruded under similar processing conditions (*e.g.*, same number of multipliers), similar fiber dimensions were expected. This size range is similar to those of PLA/PCL fibers obtained from electrospinning[29] and is ideal for many biomedical applications, such as tissue engineering scaffolds. Any slight variations in fiber dimensions may have been caused by processing differences induced by the collection of the composite tapes from the chilled roller because PLA cools more rapidly than PCL and can adhere to the surface of the roller.[30]

Table 1. Dimensions of PLA and PCL Fibers[a]

system	width (μm)	thickness (μm)
100 PLA/0 PCL	0.23 ± 0.1	0.68 ± 0.1
75 PLA/25 PCL	0.34 ± 0.1	0.23 ± 0.5
50 PLA/50 PCL	0.31 ± 0.1	0.14 ± 0.1
25 PLA/75 PCL	0.32 ± 0.1	0.19 ± 0.1
0 PLA/100 PCL	0.43 ± 0.1	0.22 ± 0.5

[a]Fibers obtained were ~300 nm in width and ~200 nm in thickness. However, the PLA fibers were measured to have an increase in thickness, likely caused by the rapid cooling of PLA that adhered to the surface of the steel roller.

Morphological Considerations. An etching study was conducted to evaluate the morphology of the PLA/PCL fiber blends in order to selectively remove one phase. Because of the rigidity of PLA, a solvent that would selectively remove the more flexible PCL was chosen to provide a more accurate representation of the initial morphology. The 75/25 and 50/50 PLA/PCL blended fibers were placed in a THF atmosphere for 25 min and then washed with methanol before drying overnight.[12] The etched morphology of the PLA/PCL fiber blends was then visualized utilizing SEM (Figure 4). For the 75 PLA/25 PCL blend, spherical voids (~50 nm in diameter) were observed, indicating a droplet-in-matrix morphology. A different blend microstructure was observed in the 50 PLA/50 PCL extruded fiber. The etched PCL phase appeared interconnected with a roughened surface texture, suggesting that PCL droplets elongated and a cocontinuous morphology emerged. A similar cocontinuous microstructure was observed for electrospun 50 PLA/50 PCL fibers.[19] To etch away the minor PLA phase in the 25 PLA/75 PCL system, the extruded fibers were submerged in acetic acid for 1 min and dried overnight. In this system, a droplet-in-matrix morphology was also noted, mirroring the 75 PLA/25 PCL blend, but consisting of a major phase of PCL and droplets of PLA. Interestingly, the droplets formed by PLA (~100 nm) were much larger than the droplets formed by PCL (~50 nm). This change in droplet size is likely due to drastic differences in crystallization temperature. PLA crystallizes at a much higher temperature than PCL ($T_{c,PLA}$ = 100 °C and $T_{c,PCL}$ = 35 °C), and as a result, the major phase provided more mobility, thus allowing the PLA to droplets to coalesce. Typical PLA/PCL blended films do form droplet-in-matrix-type morphologies when phases are not equally blended together.[9,31,32] The morphological results are similar to those seen in previous studies of PLA/PCL blends, indicating that blend composition has a distinct influence on micro/nanoscale phases that will likely impact bulk material performance.[12]

Crystalline Domain. Initial analysis of the microstructure was achieved by measuring the crystallinity of the PLA and the PCL phases. The endothermic phase transitions (Table S2, Figure S3) were obtained from the first heating cycle in DSC (Figure 5). This is different from the typical characterization performed on electrospun fibers because the thermal histories

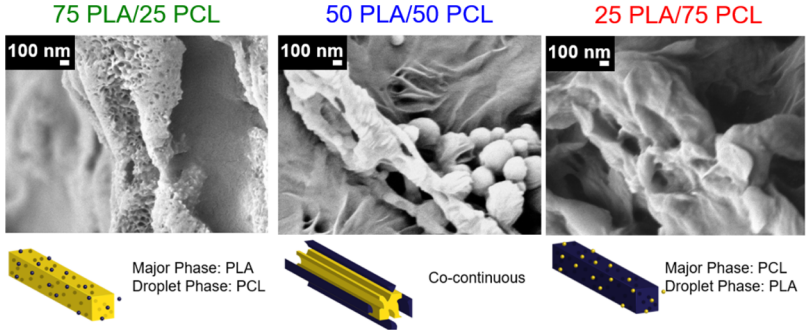

Figure 4. (Above) SEM micrographs of blend systems after selective etching of a single phase. (Below) schematic representation of the etching process, where yellow refers to PLA and blue refers to PCL. The 75 PLA/25 PCL fibers were found to be droplets of PCL, encased in a matrix of PLA. The 50 PLA/50 PCL fibers exhibited a cocontinuous morphology. The 25 PLA/75 PCL were observed to be droplets of PLA surrounded by a matrix of PCL. The droplets in the 75 PLA/25 PCL fibers were smaller than the droplets in the 25 PLA/75 PCL fibers, which is attributed to PLA crystallizing at a higher temperature than PCL.

https://dx.doi.org/10.1021/acs.macromol.0c00289
Macromolecules XXXX, XXX, XXX−XXX

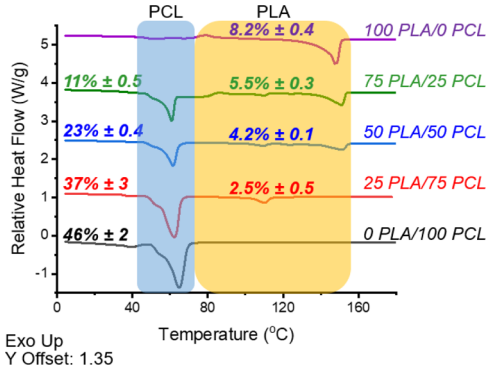

Figure 5. First DSC heating cycle, where blue refers to endothermic phase transition associated with PCL, and yellow refers to endothermic phase transitions associated with PLA.

were imprinted on the fibers during the coextrusion process. The control PLA fibers exhibited an endothermic phase transition at 150 °C with a crystallinity of ∼8.2% that accounts for the exothermic cold crystallization peak at 82 °C. A higher degree of crystallinity (∼46%) was calculated for the control PCL fibers at an endothermic phase transition at 61 °C. This overlapped with the glass transition temperature of PLA, and consequently, the glass transition temperature for the PLA phase in the blended system was not observed. As expected, the thermal behavior of the PLA/PCL fibers was influenced by the weight ratio of the blends. The PLA crystallinity decreased, while the PCL crystallinity increased as the PLA content was reduced. The 75 PLA/25 PCL fibers exhibited melting peaks consistent with both the control PLA and PCL transitions and the emergence of a broad, bimodal endothermic peak centered at ∼110 °C. We attribute this new thermal transition to fractionated crystallization.[33,34] Here, the crystalline domain of the minor component within an immiscible blend may be depressed and display bimodal character because of varying nucleation points. This behavior occurs when a semicrystalline polymer is morphologically confined within an immiscible blend; the interface between phases and the bulk both act as nucleating agents. Additionally, these nucleating points have different efficiencies; thus, fractionated crystallization can occur.[21,35−37] Utilizing the associated enthalpy of fusion for PLA (75.6 J/g) and PCL (139 J/g), crystallinity values of 5.5% (PLA) and 11% (PCL) were calculated for this PCL droplet-in-PLA matrix morphology with ∼50 nm diameter PCL droplets. For the cocontinuous 50 PLA/50 PCL system, the PCL crystallinity increased to 23%, while the PLA crystalline fraction decreased to 4.2%. Similar to the 75 PLA/25 PCL blended fibers, the PLA endotherm transition was quite broad, and multiple, broad peaks between 110 and 120 °C, attributed to fractionated crystallization, were apparent. The cold crystallization peak for PLA also disappears, suggesting that at this composition, PCL aids in nucleation of PLA.[36] For the 25 PLA/75 PCL fiber blends with a droplet-in-matrix morphology, melting transitions were observed at ∼65 °C, consistent with the control PCL peak; however, the emergent melting transition at ∼110 °C was the only endothermic peak observed in the PLA region. The PCL crystallinity increased to 37%, as expected, while the PLA crystallinity was ∼2.5% in these larger PLA aggregates. This decrease in crystallinity, which has been previously observed in PLA/PCL electrospun fibers,[38] indicates that large-scale homogeneous nucleation was prevented in each phase.[39,40] Additionally, the endothermic phase transition of PLA was depressed with PCL as the major blend component. This depressed melt temperature occurs at the same temperature as one of the melt transitions the 50 PLA/50 PCL fibers exhibited, which was attributed to fractionated crystallization.[37]

To further probe changes in the size of crystallites of the PLA/PCL extruded nonwoven fibers, WAXS was utilized. It is important to note that X-ray scattering was not used to quantify crystallinity owing to the heterogeneity of the nonwoven fiber mats.[41,42]

The narrowing or broadening of an individual WAXS peak reflection provides information about packing within a crystalline domain, where a broader peak indicates a decrease in the orthogonal size of the crystallite.[43] This relationship can be quantified (eq 2) using the Scherrer formula.[44]

$$L_{hkl} = \frac{K\lambda}{B_{hkl}\cos\theta_{hkl}} \quad (2)$$

Here, the average domain size of the crystallite (L_{hkl}) is correlated to a shape factor (K), which is typically 0.89 for polymers, the full width at half-maximum (B_{hkl}) of a specific crystal reflection, the Bragg angle for that reflection (θ), and wavelength (λ).[25] To obtain the B_{hkl} for the peaks, a Lorentzian fit was utilized.

Two distinct crystal reflections were selected to differentiate the PLA and the PCL phases in the PLA/PCL fibers (Figure 6). The (110)/(200) crystal reflection at 1.19 Å^{-1} was used to

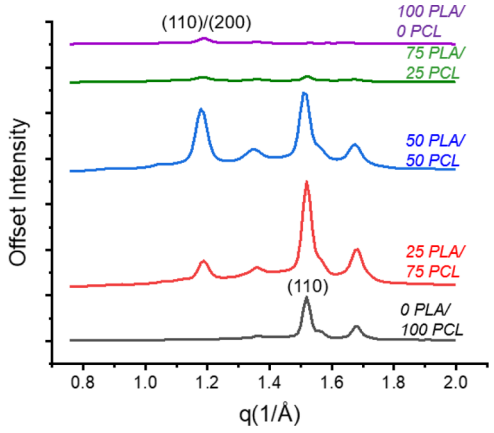

Figure 6. One-dimensional WAXS curves of PLA/PCL fibers. Two isolated reflections were identified that correspond to the two components of the blends: (110)/(200) PLA and (110) PCL.

characterize PLA crystallites, and the (110) crystal reflection at 1.52 Å^{-1} was used for PCL crystallites.[25,45] Here, it is important to note that all reflections detected occur at the same q value, and no new reflections are observed. The B_{hkl} and corresponding L_{hkl} for each reflection was calculated to determine the relationship between blend composition and the mean crystallite size (Table 2). Using the (110)/(200) crystal reflection, a L_{hkl} of 35 Å was calculated for the control PLA fibers. For the control PCL fibers, a L_{hkl} of 48 Å at the (110) crystal reflection was determined. The L_{hkl} values for the 75 PLA/25 PCL fiber blends were 11 and 30 Å for the PLA and PCL reflection, respectively. The PLA L_{hkl} significantly decreased (∼3×) compared to the control PLA fiber, suggesting that the PCL droplets limit the growth of PLA crystalline domains. The L_{hkl} value of the PCL domain is also

https://dx.doi.org/10.1021/acs.macromol.0c00289
Macromolecules XXXX, XXX, XXX−XXX

Table 2. One-Dimensional B_{hkl} and L_{hkl} Values Calculated for the Two Reflections[a]

system	B_{hkl} (110)/(200)	B_{hkl} (110)	L_{hkl} (110)/(200) (Å)	L_{hkl} (110) (Å)
100 PLA/0 PCL	0.039		35	
75 PLA/25 PCL	0.12	0.047	11	30
50 PLA/50 PCL	0.043	0.045	32	31
25 PLA/75 PCL	0.035	0.034	39	41
0 PLA/100 PCL		0.029		48

[a]At the (110)/(200) reflection, the B_{hkl} decreased in the blended fibers as the PCL content increased, indicating an increase in the mean crystallite size. However, the B_{hkl} decreased as the PLA content increased, suggesting a decrease in the mean crystallite size.

smaller (~2×) than that of the control PCL fibers. For the cocontinuous 50 PLA/50 PCL blended fibers, the mean PCL crystallite size (L_{hkl} = 31 Å) is similar to that of the 75 PLA/25 PCL fiber blends, but the PLA phase exhibits a significant increase in the size of the crystalline domain (32 Å). For the 25 PLA/75 PCL fibers, the PLA crystallite size increases (39 Å), while the PCL crystalline domain size is only slightly decreased (L_{hkl} = 41 Å) compared to that of the control PLA. These findings suggest that PCL accelerated nucleation growth of the PLA crystallites, but PLA inhibited the nucleation of PCL crystallites. Additionally, the changes in the crystallite size may have been a result of morphological confinement imparted on the PLA and PCL phases.[46]

Mechanical Analysis. With insight into the morphology and crystallinity of the PLA/PCL fiber blends, the mechanics of these rectangular PLA/PCL fibers were probed *via* tensile testing, where each system was uniaxially deformed until failure. The void fraction of the nonwoven mat was considered to obtain a true cross-sectional area for each tensile measurement. Failure was characterized as the point at which a reduction of 90% of the maximum force was measured (Figure 7, Table 3). This approach was taken to account for the heterogeneous nature of these nonwoven, control, and PLA/PCL fibers. Rupture of individual fibers is nonuniform, leading to heterogeneity in the tensile curves, especially for the control PCL fibers.[47] It is initially apparent that the PLA fibers exhibited brittle-like behavior because of their glass transition temperature (T_g = 59 °C) with limited extensibility (7.0 ± 2.3%), a yield stress of 1641 ± 57.4 MPa, and a Young's modulus of 61.8 ± 8.6 MPa, corresponding to a low toughness (0.71 ± 0.18 MJ/m^3). In contrast, the control PCL fibers were quite tough (2150 ± 520 MJ/m^3) because of their exceptional extensibility (1600 ± 160%) and a moderate Young's modulus (52.9 ± 6.4 MPa). Additionally, the PCL control displayed the highest yield stress of 4577 ± 481 MPa. However, it is well-reported that PLA/PCL blends undergo phase separation and that this microstructure impacts the mechanics of the blend.[19,48−50] As a result of this phase separation, the PLA/PCL fibers exhibited mechanical properties that were not simply averages of the individual PLA and PCL components.

Despite the droplet-in-PLA matrix morphology of PCL, the 75 PLA/25 PCL blended fibers exhibit a low Young's modulus (6.19 ± 23 MPa) with only limited extensibility (29 ± 1.5%), leading to low toughness (0.337 ± 0.042 MJ/m^3) and the lowest yield stress (246.5 ± 12.5 MPa). This mechanical behavior, which differs considerably from both the control PCL and PLA fibers, is likely due to the poor interfacial adhesion that is often observed in these phase-separated blends[51] and the reduction in crystallinity[52] for both the PLA and PCL phases. In the cocontinuous 50 PLA/50 PCL fiber blends, the mechanical properties, including Young's modulus (30.0 ± 7.9 MPa), elongation-at-break (230 ± 39%), yield stress (1916 ± 371 MPa), and toughness (71.4 ± 19 MJ/m^3), are significantly higher than those of the 75 PLA/25 PCL fibers. It is likely that this balance in mechanical response is due to the nucleation and growth mechanisms of the PLA and PCL domains observed in the WAXS analysis and the synergistic nature of the microstructure.[53] A slight reduction in the mechanical behavior is observed for the PLA droplet-in-PCL matrix fibers (25 PLA/75 PCL) with a Young's modulus of 26.9 ± 0.95 MPa, an elongation-at-break of 160 ± 42%, and yield stress (1621 ± 128 MPa), leading to a toughness value of 63.0 ± 75 MJ/m^3. The larger PLA droplet size observed *via* etching for this fiber blend composition may also play a role in the reduction of mechanics, although the flexible PCL matrix aided in the observed overall toughness. Interestingly, two of the compositions of PLA/PCL blended fibers (the two with larger PCL content) exhibit higher toughness values, but lower moduli than those of the control PLA fibers, which was attributed to the decrease in crystallinity.[54,55]

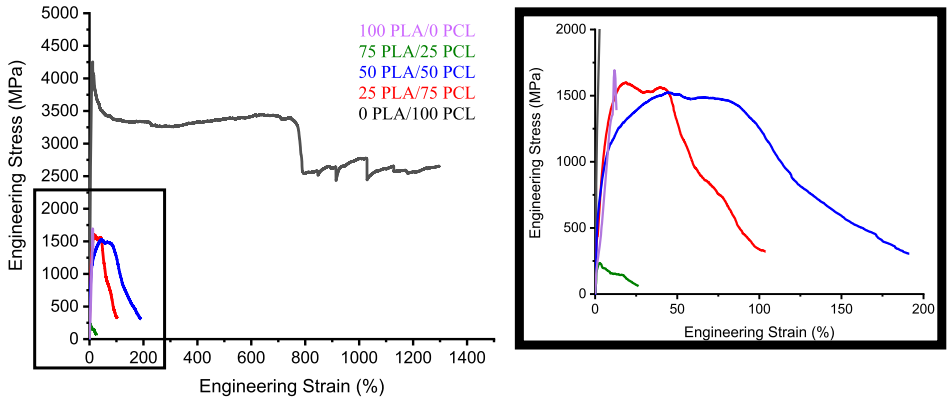

Figure 7. Tensile curve of PLA/PCL fibers. Left: Full curve of all systems. Right: Inset of curve PLA control fibers exhibit a brittle-like behavior, and PCL control fiber behavior is more rubber-like. On increasing the PCL component within the blends, the behavior of PLA/PCL fibers is more ductile than that of the PLA control fibers.

https://dx.doi.org/10.1021/acs.macromol.0c00289
Macromolecules XXXX, XXX, XXX−XXX

Table 3. Summary of the Mechanical Properties of Control PLA and PCL and PLA/PCL Fiber Blends

system	toughness (MJ/m^3)	Young's modulus (MPa)	elongation (%)	yield stress (MPa)
100 PLA/0 PCL	0.71 ± 0.18	62 ± 8.6	7.0 ± 2.3	1641 ± 57.4
75 PLA/25 PCL	0.34 ± 0.042	6.2 ± 23	29 ± 1.5	246.5 ± 12.5
50 PLA/50 PCL	71 ± 19	30.0 ± 7.9	230 ± 39	1916 ± 372
25 PLA/75 PCL	63 ± 7.5	27 ± 0.95	160 ± 43	1621 ± 128
0 PLA/100 PCL	2200 ± 520	53 ± 6.4	1600 ± 160	4577 ± 481

CONCLUSIONS

A high throughput processing method, multilayer coextrusion, was utilized to fabricate PEO/polyester composite tapes, where the polyester phase was a blend of PLA/PCL. A three-step wash, delamination, and wash protocol was implemented to remove ≥89.9 wt % of the PEO matrix. The dimensions of the extruded, rectangular nonwoven fibers were ∼300 nm wide and ∼200 nm thick. The morphologies of the PLA/PCL blends were determined by selectively removing one phase of the blend, and SEM was used to image the etched fibers. Droplet-in-matrix microstructures were observed for the 75 PLA/25 PCL and 25 PLA/75 PCL fiber blends, while the 50 PLA/50 PCL fiber blends were cocontinuous. The morphological effects on the crystalline domains and mechanics were then explored. DSC analysis showed that blending of semicrystalline PLA and PCL leads to a reduction in the crystallinity in each phase as well as a broadening and shift of the PLA endothermic peak, as a result of fractionated crystallization. Further WAXS analysis detailed an influence of the mean size of the crystallites. The PLA crystallites increased in size with increasing PCL content, suggesting that PCL encouraged PLA growth. However, the PCL crystalline domain size reduced upon increasing the PLA fraction, suggesting an influence on PCL nucleation. These changes in the crystalline phase and the morphology played a key role in the bulk mechanics of the system. Interestingly, the PLA/PCL blends exhibited a reduction in moduli compared to the two controls. However, a significant increase in toughness was observed when PLA was blended with increasing amounts of PCL. The 50 PLA/50 PCL blend displayed synergistic mechanical properties with a moderate modulus and high extensibility. This combination lead to a tough fiber blend, which was attributed to the cocontinuous morphology. While other studies focus on compatibilization between the PLA and PCL phases, this research draws important connections between morphology, crystallinity, and mechanical properties of the PLA/PCL blend fibers, which can be utilized to understand degradation behavior in the design space of biomedical scaffolding. The influence of fiber blend architecture (*i.e.* rectangular) *via* a melt-based coextrusion approach is yet to be explored. The results described herein establish that this novel processing method yields materials with similar properties to what is already known regarding polymer blends. However, the processing method produces fibers with significantly higher surface areas and improved scalability when compared to solvent-based processing methods. This work demonstrates that multilayer coextrusion can be utilized to fabricate fibers with tailored mechanical properties with the potential to impact biomedical applications, such as tissue engineering, where specific tissues require a distinct mechanical profile.

ASSOCIATED CONTENT

Supporting Information

The Supporting Information is available free of charge at https://pubs.acs.org/doi/10.1021/acs.macromol.0c00289.

Fiber purity calculations, isolated fiber mats, fiber dimensions, void fraction calculations, and thermal behavior obtained from DSC (PDF)

AUTHOR INFORMATION

Corresponding Authors

Jonathan K. Pokorski − *Department of Nanoengineering and Institute for Materials Discovery and Design, University of California San Diego, La Jolla, California 92093, United States;* orcid.org/0000-0001-5869-6942; Phone: (858) 246-3183; Email: jpokorski@ucsd.edu

LaShanda T. J. Korley − *Department of Materials Science and Engineering and Department of Chemical and Biomolecular Engineering, University of Delaware, Newark, Delaware 19716, United States;* orcid.org/0000-0002-8266-5000; Phone: (302) 831-0937; Email: lkorley@udel.edu

Author

Kris M. Van de Voorde − *Department of Materials Science and Engineering, University of Delaware, Newark, Delaware 19716, United States;* orcid.org/0000-0003-3398-2664

Complete contact information is available at: https://pubs.acs.org/10.1021/acs.macromol.0c00289

Notes

The authors declare no competing financial interest.

ACKNOWLEDGMENTS

The authors acknowledge funding from the National Science Foundation (NSF—OISE 1844463) PIRE: Bio-inspired Materials and Systems and funding to K.M.V. through the NSF Graduate Research Fellowship Program. The Advanced Materials Characterization Laboratory (AMCL) and the Keck Microscopy Center at the University of Delaware are acknowledged for providing access to thermal and morphological characterization instrumentation. The authors appreciate the use of multilayer coextrusion facilities in the NSF STC Center for Layered Polymeric Systems (CLiPS) (grant DMR-0423914) at Case Western Reserve University.

REFERENCES

(1) Jaratrotkamjorn, R.; Khaokong, C.; Tanrattanakul, V. Toughness Enhancement of Poly(Lactic Acid) by Melt Blending with Natural Rubber. *J. Appl. Polym. Sci.* **2011**, *124*, 5027−5036.

(2) Yeo, J. H.; Lee, C. H.; Park, C.-S.; Lee, K.-J.; Nam, J.-D.; Kim, S. W. Rheological, Morphological, Mechanical, and Barrier Properties of PP/EVOH Blends. *Adv. Polym. Technol.* **2001**, *20*, 191−201.

(3) Small, J. D. Multicomponent polyester/polycarbonate blends with improved impact strength and processability. 2130907 A1, 1993, No. 19.

(4) Arias, V.; Höglund, A.; Odelius, K.; Albertsson, A.-C. Tuning the Degradation Profiles of Poly(L-Lactide)-Based Materials through Miscibility. *Biomacromolecules* **2014**, *15*, 391−402.
(5) Farheen, S.; Jahan, F.; Inamdar, H. K.; Mathad, R. D. Effect Of Polymer Blending On Mechanical And Thermal Properties. *Indian J. Sci. Res.* **2015**, *12*, 520−522.
(6) Rengier, F.; Mehndiratta, A.; von Tengg-Kobligk, H.; Zechmann, C. M.; Unterhinninghofen, R.; Kauczor, H.-U.; Giesel, F. L. 3D printing based on imaging data: review of medical applications. *Int J. Comput. Ass. Rad. Sur.* **2010**, *5*, 335−341.
(7) Slomkowski, S. Biodegradable Polyesters for Tissue Engineering. *Macromol. Symp.* **2007**, *253*, 47−58.
(8) O'Brien, F. J. Biomaterials & Scaffolds for Tissue Engineering. *Mater. Today* **2011**, *14*, 88−95.
(9) Eguiaz, I.; Urquijo, J.; Guerrica-echevarr, G. Melt Processed PLA/PCL Blends: Effect of Processing Method on Phase Structure, Morphology, and Mechanical Properties. *J. Appl. Polym. Sci.* **2015**, *132*, 42641.
(10) Finniss, A.; Agarwal, S.; Gupta, R. Retarding Hydrolytic Degradation of Polylactic Acid: Effect of Induced Crystallinity and Graphene Addition. *J. Appl. Polym. Sci.* **2016**, *133*, 44166.
(11) Ventola, C. L. Medical Applications for 3D Printing: Current and Projected Uses. *Pharm Ther.* **2014**, *39*, 704−711.
(12) Ostafinska, A.; Fortelny, I.; Nevoralova, M.; Hodan, J.; Kredatusova, J.; Slouf, M. Synergistic Effects in Mechanical Properties of PLA/PCL Blends with Optimized Composition, Processing, and Morphology. *RSC Adv.* **2015**, *5*, 98971−98982.
(13) Megelski, S.; Stephens, J. S.; Chase, D. B.; Rabolt, J. F. Micro- and Nanostructured Surface Morphology on Electrospun Polymer Fibers. *Macromolecules* **2002**, *35*, 8456−8466.
(14) Kim, S. E.; Wang, J.; Jordan, A. M.; Korley, L. T. J.; Baer, E.; Pokorski, J. K. Surface Modification of Melt Extruded Poly(ε-Caprolactone) Nano Fi Bers: Toward a New Scalable Biomaterial Scaffold. *ACS Macro Lett.* **2014**, *3*, 585−589.
(15) Pham, Q. P.; Sharma, U.; Mikos, A. G. Electrospinning of Polymeric Nanofibers for Tissue Engineering Applications: A Review. *Tissue Eng.* **2006**, *12*, 1197−1211.
(16) Jordan, A. M.; Viswanath, V.; Kim, S.-E.; Pokorski, J. K.; Korley, L. T. J.; Jordan, A. M.; Jordan, A. M.; Kim, S. Processing and Surface Modification of Polymer Nanofibers for Biological Scaffolds : A Review. *J. Mater. Chem. B* **2016**, *4*, 5958−5974.
(17) Schiffman, J. D.; Schauer, C. L. A Review : Electrospinning of Biopolymer Nanofibers and Their Applications A Review : Electrospinning of Biopolymer Nanofibers and Their Applications. *Polym. Rev.* **2008**, *48*, 317.
(18) Scaffaro, R.; Lopresti, F.; Botta, L. Preparation , Characterization and Hydrolytic Degradation of PLA/PCL Co-Mingled Nano Fibrous Mats Prepared via Dual-Jet Electrospinning. *Eur. Polym. J.* **2017**, *96*, 266−277.
(19) Lu, L.; Wu, D.; Zhang, M.; Zhou, W. Fabrication of Polylactide/Poly(ε-caprolactone) Blend Fibers by Electrospinning: Morphology and Orientation. *Ind. Eng. Chem. Res.* **2012**, *51*, 3682−3691.
(20) Thavasi, V.; Singh, G.; Ramakrishna, S. Electrospun Nanofibers in Energy and Environmental Applications. *Energy Environ. Sci.* **2008**, *1*, 205−221.
(21) Fenni, S. E.; Wang, J.; Haddaoui, N.; Favis, B. D.; Müller, A. J.; Cavallo, D. Crystallization and Self-Nucleation of PLA, PBS and PCL in Their Immiscible Binary and Ternary Blends. *Thermochim. Acta* **2019**, *677*, 117−130.
(22) Tabi, T.; Sajo, I. E.; Szabo, F.; Luyt, A. S.; Kovacs, J. G. Crystalline structure of annealed polylactic acid and its relation to processing. *Express Polym. Lett.* **2010**, *4*, 659−668.
(23) Jenkins, M. J.; Harrison, K. L. The Effect of Molecular Weight on the Crystallization Kinetics of Polycaprolactone. *Polym. Adv. Technol.* **2006**, *17*, 474−478.
(24) Nijenhuis, A. J.; Colstee, E.; Grijpma, D. W.; Pennings, A. J. High molecular weight poly(L-lactide) and poly(ethylene oxide) blends: thermal characterization and physical properties. *Polymer* **1996**, *37*, 5849−5857.
(25) Jordan, A. M.; Korley, L. T. J. Toward a Tunable Fibrous Scaffold: Structural Development during Uniaxial Drawing of Coextruded Poly(ε-caprolactone) Fibers. *Macromolecules* **2015**, *48*, 2614−2627.
(26) Jordan, A. M.; Marotta, T.; Korley, L. T. J. Reducing Environmental Impact: Solvent and PEO Reclamation During Production of Melt-Extruded PCL Nanofibers. *ACS Sustain. Chem. Eng.* **2015**, *3*, 2994−3003.
(27) Durigon, P. E. R.; Petri, D. F. S.; Drings, H.; Schimmel, T.; Bruns, M. Characterization and Modification of Polymer Blend Films. *Colloid Polym. Sci.* **2001**, *279*, 1013−1019.
(28) Yazgan, G.; Dmitriev, R. I.; Tyagi, V.; Jenkins, J.; Rotaru, G.-M.; Rottmar, M.; Rossi, R. M.; Toncelli, C.; Papkovsky, D. B.; Maniura-Weber, K.; Fortunato, G. Steering surface topographies of electrospun fibers: understanding the mechanisms. *Sci. Rep.* **2017**, *7*, 158.
(29) Kumbar, S. G.; James, R.; Nukavarapu, S. P.; Laurencin, C. T. Electrospun nanofiber scaffolds: engineering soft tissues. *Biomed. Mater.* **2008**, *3*. DOI: DOI: 10.1088/1748-6041/3/3/034002.
(30) Zhang, C.; Lan, Q.; Zhai, T.; Nie, S. Melt Crystallization Behavior and Crystalline Morphology of Polylactide/Poly(ε-caprolactone) Blends Compatibilized by Lactide-Caprolactone Copolymer. *Polymers* **2018**, *10*, 1181.
(31) Gardella, L.; Calabrese, M.; Monticelli, O. PLA maleation: an easy and effective method to modify the properties of PLA/PCL immiscible blends. *Colloid Polym. Sci.* **2014**, *292*, 2391−2398.
(32) Wu, D.; Zhang, Y.; Zhang, M.; Zhou, W. Phase Behavior and Its Viscoelastic Response of Polylactide/Poly(ε-Caprolactone) Blend. *Eur. Polym. J.* **2008**, *44*, 2171−2183.
(33) As'habi, L.; Hassan, S.; Ali, H.; Häussler, L.; Wagenknecht, U.; Heinrich, G. Non-Isothermal Crystallization Behavior of PLA/LLDPE/Nanoclay Hybrid: Synergistic Role of LLDPE and Clay. *Thermochim. Acta* **2013**, *565*, 102−113.
(34) Ghijsels, A.; Groesbeek, N.; Yip, C. Multiple Crystallization Behaviour of Polypropylene/Thermoplastic Rubber Blends and Its Use in Assessing Blend Morphology. *Polymer* **1982**, *23*, 1913−1916.
(35) Morales, R. A.; Arnal, M. L.; Müller, A. J. The Evalulation of the State of Dispersion in Immicible Blends Where the Minor Phase Exhibits Fractionated Crystallization. *Polym. Bull.* **1995**, *35*, 379−386.
(36) Jia, S.; Yu, D.; Zhu, Y.; Wang, Z.; Chen, L.; Fu, L. Morphology, Crystallization and Thermal Behaviors of PLA-Based Composites: Wonderful Effects of Hybrid GO/PEG via Dynamic Impregnation. *Polymers* **2017**, *9*, 528.
(37) Michell, R. M.; Blaszczyk-lezak, I.; Mijangos, C.; Müller, A. J. Confinement Effects on Polymer Crystallization: From Droplets to Alumina Nanopores. *Polymer* **2013**, *54*, 4059−4077.
(38) Haroosh, H. J.; Chaudhary, D. S.; Dong, Y. Electrospun PLA/PCL Fibers with Tubular Nanoclay : Morphological and Structural Analysis. *J. Appl. Polym. Sci.* **2011**, *124*, 3930−3939.
(39) Wurm, A.; Zhuravlev, E.; Eckstein, K.; Jehnichen, D.; Pospiech, D.; Androsch, R.; Wunderlich, B.; Schick, C. Crystallizationon and Homogeneous Nucleation Kinetics of Poly(ε-caprolactone) (PCL) with Different Molar Masses. *Macromolecules* **2012**, *45*, 3816−3828.
(40) Yeh, J.-T.; Wu, C.-J.; Tsou, C.-H.; Chai, W.-L.; Chow, J.-D.; Huang, C.-Y.; Chen, K.-N.; Wu, C.-S. Study on the Crystallization, Miscibility, Morphology, Properties of Poly(lactic acid)/Poly(ε-caprolactone) Blends. *Polym. Plast. Technol. Eng.* **2009**, *48*, 571−578.
(41) Mousa, A.; Kusminarto, K.; Suparta, G. B. A New Simple Method to Measure the X-Ray Linear Attenuation Coefficients of Materials Using Micro-Digital Radiography Machine. *Int. J. Appl. Eng. Res.* **2017**, *12*, 10589−10594.
(42) De Jeu, W. H. *Basic X-Ray Scattering for Soft Matter*, 1st Ed.; Oxford University Press: New York, 2016.
(43) Campbell, D.; Pethrick, R.; White, J. *Polymer Characterization*, 2nd Ed.; Stanley Thornes: Cheltenham, 2000; pp 194−236.
(44) Patterson, A. L. The Scherrer Formula for X-Ray Particle Size Determination. *Phys. Rev.* **1939**, *56*, 978−982.

https://dx.doi.org/10.1021/acs.macromol.0c00289
Macromolecules XXXX, XXX, XXX−XXX

(45) Rezgui, F.; Swistek, M.; Hiver, J. M.; G'Sell, C.; Sadoun, T. Deformation and Damage upon Stretching of Degradable Polymers (PLA and PCL). *Polymer* **2005**, *46*, 7370−7385.
(46) Yu, C.; Xie, Q.; Bao, Y.; Shan, G.; Pan, P. Crystalline and Spherulitic Morphology of Polymers Crystallized in Confined Systems. *Crystals* **2017**, *7*, 147.
(47) Mueller, D. H.; Kochmann, M. Numerical Modeling of Thermobonded Nonwovens. *J. Eng. Fibers Fabr.* **2004**, *13*, 56−62.
(48) Todo, M.; Park, S.-D.; Takayama, T.; Arakawa, K. Fracture Micromechanisms of Bioabsorbable PLLA/PCL Polymer Blends. *Eng. Fract. Mech.* **2007**, *74*, 1872−1883.
(49) Patrício, T.; Bártolo, P. Thermal Stability of PCL/PLA Blends Produced by Physical Blending Process. *Procedia Eng.* **2013**, *59*, 292−297.
(50) Suzuki, Y.; Duran, H.; Akram, W.; Steinhart, M.; Floudas, G.; Butt, H.-J. Multiple Nucleation Events and Local Dynamics of Poly(ε-Caprolactone) (PCL) Confined to Nanoporous Alumina. *Soft Matter* **2013**, *9*, 9189.
(51) Broz, M.; Vanderhart, D. L.; Washburn, N. R. Structure and Mechanical Properties of Poly (D ,L -Lactic Acid)/Poly(ε-Caprolactone) Blends. *Biomaterials* **2003**, *24*, 4181−4190.
(52) Bessell, T. J.; Hull, D.; Shortall, J. B. The Effect of Polymerization Conditions and Crystallinity on the Mechanical Properties and Fracture of Spherulitic Nylon 6. *J. Mater. Sci.* **1975**, *10*, 1127−1136.
(53) Joseph, S.; Thomas, S. Modeling of Tensile Moduli in Polystyrene / Polybutadiene Blends. *J. Polym. Sci., Part B: Polym. Phys.* **2002**, *40*, 755−764.
(54) Pongtanayut, K.; Thongpin, C.; Santawitee, O. The Effect of Rubber on Morphology, Thermal Properties and Mechanical Properties of PLA/NR and PLA/ENR Blends. *Energy Procedia* **2013**, *34*, 888−897.
(55) Jiao, L.; Huang, C.-L.; Zeng, J.-B.; Wang, Y.-Z.; Wang, X.-L. Thermochimica Acta Miscibility , Crystallization and Mechanical Properties of Biodegradable Blends of Poly (l -Lactic Acid) and Poly (Butylene Succinate-b-Ethylene Succinate) Multiblock Copolymer. *Thermochim. Acta* **2012**, *539*, 16−22.

https://dx.doi.org/10.1021/acs.macromol.0c00289
Macromolecules XXXX, XXX, XXX−XXX